

Current Density Contribution to Plasmonic Enhancement Effects in Metal–Semiconductor–Metal Photodetectors

Ahmad A. Darweesh , Stephen J. Bauman , David A. French, Ahmad Nusir , *Student Member, IEEE*,
Omar Manasreh , *Senior Member, IEEE*, and Joseph B. Herzog 

Abstract—This work studies how the local current density in a metal–semiconductor–metal photodetector (MSM PD) corresponds to the plasmonic enhancement and therefore affects the overall enhancement of the device. For this type of semiconductor photodetector, the enhancement of incident light due to plasmonic structures is most critical inside the substrate, where the photocurrent is generated. This work develops a relationship between the total device optical enhancement and the current density by considering the average optical enhancement, weighted by the current density in the GaAs layer of a simulated MSM PD. This corresponds to an increased overall current in the device. Effects of the wire and nanoslit widths on the total weighted optical enhancement were studied. The results showed that both widths have a significant impact on the total weighted optical enhancement, improving it by two orders of magnitude when using the smallest possible wire widths and nanoslits.

Index Terms—Current density, MSM photodetector, nanoslit, nanogap, plasmonic.

I. INTRODUCTION

WHEN light of a specific wavelength illuminates a metal (gold, for example), it will interact with the electrons in the conduction band, causing them to oscillate with a particular corresponding frequency.

Manuscript received October 16, 2017; revised January 25, 2018; accepted February 26, 2018. Date of publication March 8, 2018; date of current version March 30, 2018. This work was supported by the University of Arkansas through the Department of Physics and the Microelectronics-Photonics Graduate Program via the Fulbright College of Arts and Sciences and the Vice Provost for Research and Economic Development as well as the Department of Electrical Engineering via the College of Engineering. The work of A. A. Darweesh was supported by the Iraqi Ministry of Higher Education and Scientific Research. The work of S. J. Bauman was supported by the Doctoral Academy Fellowship through the University of Arkansas Graduate School. (*Corresponding author: Joseph B. Herzog*.)

A. A. Darweesh and S. J. Bauman are with the Microelectronics-Photonics Program, University of Arkansas, Fayetteville, AR 72701 USA (e-mail: aadarwee@uark.edu; sjbauman@uark.edu).

D. A. French is with the Department of Physics, University of Arkansas, Fayetteville, AR 72701 USA (e-mail: daf001@uark.edu).

A. Nusir and O. Manasreh are with the Department of Electrical Engineering, University of Arkansas, Fayetteville, AR 72701 USA (e-mail: ainusir@uark.edu; manasreh@uark.edu).

J. B. Herzog is with the Department of Physics, Microelectronics and Photonics Program and the Institute for Nanoscience and Engineering, University of Arkansas, Fayetteville, AR 72701 USA (e-mail: jbherzog@email.uark.edu).

Color versions of one or more of the figures in this paper are available online at <http://ieeexplore.ieee.org>.

Digital Object Identifier 10.1109/JLT.2018.2811749

The collective oscillation of the electrons within the metal is called a plasmon [1]. The geometry of the metallic structure is one factor that can play a major role in the light-matter interaction [2]. It is possible to generate a strengthened local electric field near one or more nanostructures due to these plasmonic effects. These regions of increased electric field strength are known as hotspots. This phenomenon can be utilized to develop applications related to enhanced optical intensity such as photodetectors [3]–[6], photovoltaics [7]–[14], biosensors [15]–[22], terahertz antennas [23], lenses with tunable parameters [24]–[27], single-molecule detection [28]–[31] and surface-enhanced Raman spectroscopy (SERS) [32]–[34].

When it comes to high-speed optical communication systems, photo-sensing devices such as metal–semiconductor–metal (MSM), p-i-n, avalanche, and heterojunction photo-detectors (PDs) are used. Of these, the MSM PD is optimal because it is simple, easy to fabricate, and has low capacitance. This low capacitance makes MSM PDs especially attractive for high-speed optical communications, because they typically exhibit large detection bandwidths.

Due to their application in optical communications, MSM PDs have been extensively studied for many years. The majority of these studies have focused on micro-scale metallic structures [35], [36], whereas recent research investigates nanoscale MSM PD structures to take advantage of plasmonic enhancement effects [37]–[39]. One type of nanostructure used to enhance the optical signal in MSM PDs is a plasmonic grating. The light produced by the grating can be increased even further by moving the metal structures closer together, creating nanoslit spacing. Previous work has investigated the optical response of nanostucture PDs [40]–[43], however, the effects of current density in the device were not taken into consideration.

This work models a gold grating on a GaAs substrate and calculates an overall enhancement based on both the plasmonic enhancement effects in the device and the current density profile in the structure, unlike other works that just model the total optical transmission or absorption [3]–[7], [39], [40], [43]. Specifically, this approach weighs the optical electric field enhancement at each point within the PD substrate by the value of the current density at that location. In this way, regions of more optical enhancement, which cause more carrier generation, are considered as more ‘valuable’ if they also correspond to regions of high current density. It is important to consider that the

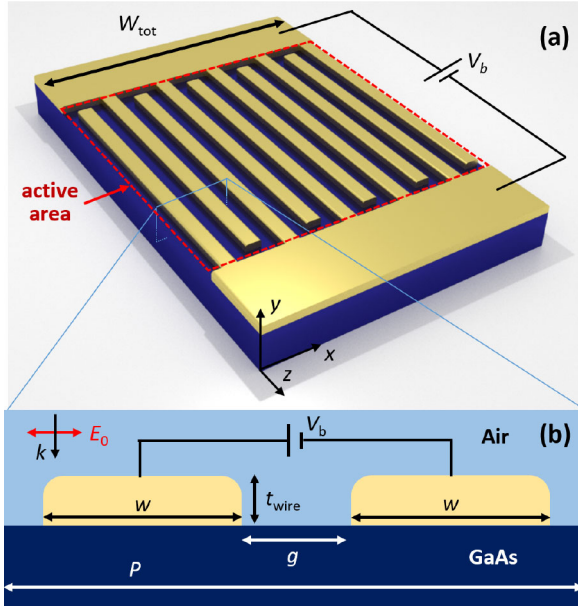


Fig. 1. Sketch of the proposed device geometry. (a) 3D depiction of the simulated MSM PD with interdigitated electrodes. GaAs was used as a substrate, and the applied bias voltage (V_b) was 5 V. (b) A cross-sectional view of one period ($P = 2w + 2g$) showing wire width (w), wire thickness (t_{wire}), and nanoslit width (g).

regions of highest current density in the GaAs are near the Au electrodes, where the electric field enhancement is also greatest due to the presence of plasmonic hotspots.

II. METHOD

A finite element method (FEM) model [44] was created to determine the optical and electrical responses for device geometries of interest. The proposed device consists of two pads containing interdigitated electrodes separated by nanoslits as shown in Fig. 1(a). Since the lengths of the interdigital electrodes are very long relative to the cross-sectional nanoscale dimensions, it is reasonable to approximate the structure as extending infinitely into and out of the page, allowing for the use of a 2D model as shown in Fig. 1(b). The electrodes were modeled on a GaAs substrate and biased at $V_b = 5$ V.

The cross-sectional view of the device has periodic boundary conditions where one period represents two nanostructure widths (w) separated by a nanoslit of width g , such that $P = 2g + 2w$, with the gold electrodes having a thickness of $t_{\text{wire}} = 15$ nm. The top edges of the nanostructures were beveled with a 5 nm radius. Light with a wavelength of 875 nm (near the bandgap energy of GaAs), linearly polarized along x , was simulated as normally incident upon the nanostructures from above. Frequency-dependent optical material properties were taken from experimental results [45], [46]. The slit width, g , is modeled down to sub-10 nm values, which can be fabricated using the previously outlined nanomasking technique [47].

The normalized electric field distribution for incident light irradiation was calculated (E_{local}/E_0), and the results are depicted in Fig. 2(a), which shows the location of plasmonic hotspots in the GaAs. This example demonstrates a grating structure with a

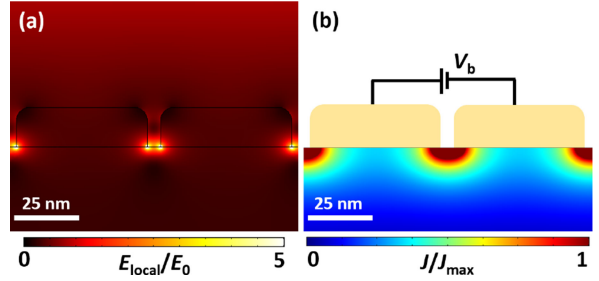


Fig. 2. Computational results. (a) Electric field enhancement distribution of one period, $P = 110$ nm, corresponding to $w = 50$ nm. (b) Current density distribution for the same period in (a).

period of 110 nm, which corresponds to $w = 50$ and $g = 5$ nm. Hotspots appear at the bottom edges of the nanostructures due to the plasmonic resonance. In addition, the normalized current density distribution (J/J_{max}) was calculated as shown in Fig. 2(b) for the same structure as in Fig. 2(a). The current density is calculated using Maxwell's equations, assuming a steady-state case and the application of a DC bias voltage. In this case, the regions of high current density are at similar locations within the substrate as those with the highest electric field enhancement. The results displayed in Fig. 2 demonstrate the key implication of the current work. Here, a weighted average optical enhancement was determined based on the local optical enhancement due to the plasmonic structures, weighted by the local current density at each calculation point.

The generation of carriers in the GaAs in regions with very low current density, due to the biasing configuration, is less significant to the overall device photocurrent than generation of carriers in high current density regions. Therefore, plasmonically enhancing the light (the number of photons), and therefore the number of carriers generated, is less significant in regions of low current density as well. Conversely, when the light is plasmonically enhanced in regions of high bias potential, and therefore high current density, the carriers generated here will contribute more significantly to the overall photocurrent of the device. This local 'enhancement significance' is treated quantitatively through a weighted average as follows.

From the results of the calculations used to create Fig. 2, the electric field (E) and current density at each point in the GaAs, E_{ij} and J_{ij} respectively, can be obtained. From these values, a weighted average optical enhancement, G_Λ , was calculated for a single period of the grating device. In this calculation, the current density was used to generate the weighted average of the optical enhancement using (1).

$$G_\Lambda = \frac{\sum [(E_{ij}/E_0)^2 J_{ij}]}{\sum J_{ij}} \quad (1)$$

The normalized optical intensity, $(E_{ij}/E_0)^2$, indicates the optical enhancement, where E_{ij} and E_0 are the local and incident electric field strengths, respectively. Thus, the field enhancement is given more weight in local substrate regions with high current density.

For a constant device area, a smaller period will mean a higher density of interdigitated finger pairs on the device. Therefore,

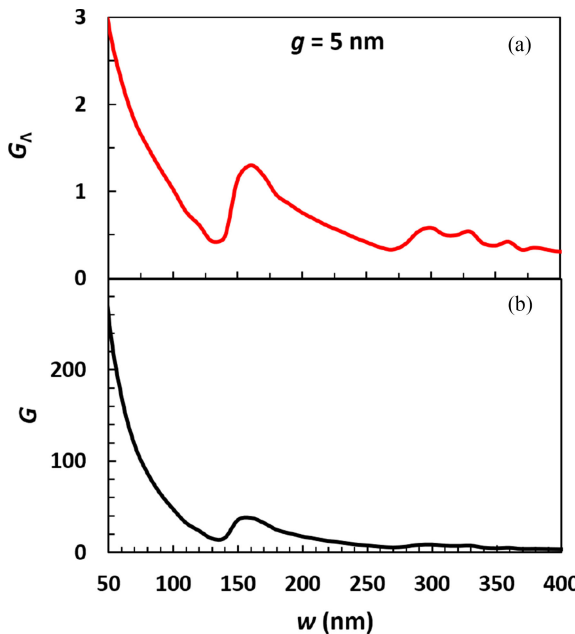


Fig. 3. Computational results. (a) Weighted optical enhancement for one period (G_A) versus w . The t_{wire} and g were fixed at 15 nm and 5 nm, respectively. (b) Total weighted optical enhancement over the device area (G) as a function of w .

for smaller periods, the overall contribution of the weighted optical enhancement per pair will be greater since more of these sections will be part of the device's active region. Each pair of electrodes adds to the total optical enhancement of the device, G , calculated by (2).

$$G = G_A \left(\frac{W_{\text{tot}}}{P} - 1 \right) \quad (2)$$

Here, $W_{\text{tot}} = 10 \mu\text{m}$ is the total width of the proposed device's active area. The effective number of periods in the active area that contribute to the total photocurrent in the device is given by $\frac{W_{\text{tot}}}{P} - 1$, where the subtraction of one corrects the calculation by neglecting the two electrodes at the edges of the full device, as no current flows at the absolute outside of the device. In this way, the weighted enhancement between each electrode is multiplied by the total number of electrodes in the full device area. The value of G corresponds to a theoretical total current-density-weighted optical enhancement, which is correlated to an increased total current in the device. Without modeling the semiconductor nature of the substrate by including parameters such as carrier generation and recombination, this approach serves to approximate the optimal MSM PD nanostructure geometry. The results, calculated via the weighted enhancement method, provide insight into the effects of plasmonic gratings on PDs and give an approximation of an ideal plasmonic structure design.

III. RESULT AND DISCUSSION

The weighted optical enhancement of one period, G_A , is plotted versus w in Fig. 3(a) using (1) for widths of w from 50 to 400 nm. The electrode thickness and spacing were held at $t_{\text{wire}} = 15$ nm and $g = 5$ nm, respectively, corresponding to

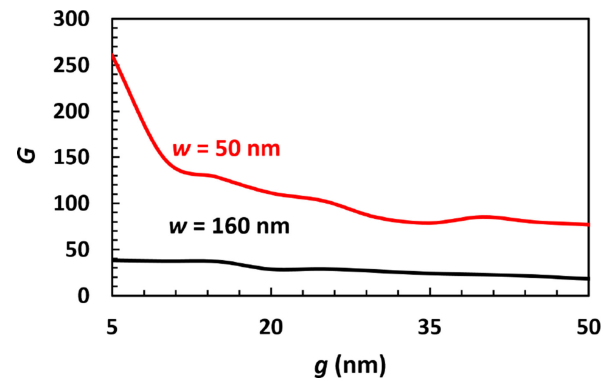


Fig. 4. Total weighted optical enhancement for the entire device (G) versus nanoslit width (g) for two different wire widths, $w = 50$ and 160 nm. The wire thickness was fixed at 15 nm, and the nanoslit was swept from 5 to 50 nm.

dimensions capable of being fabricated via nanomasking. The total weighted optical enhancement as a function of w is also plotted in Fig. 3(b).

Both the weighted optical enhancement for one period (G_A) and the total across the device area (G) increase with decreasing w . For G_A , peaks were observed over the range of w , with the maximum notable peak at $w = 160$ nm. This strong peak, as well as other peaks at higher w values, correspond to Fabry-Perot-like oscillations of the plasmonic waves resonating strongly for specific width values, similar to previous results [47]. As w decreases down to 50 nm, G_A continues to increase as the plasmonic effect increases with smaller structure sizes. The total enhancement over the entire device, G , also increases inversely with w . Since the density of electrodes increases with decreasing w , the total number of electrode pairs per unit area also increases. This effect, along with the fact that G_A increases as w decreases, leads to the larger G values occurring for smaller electrode widths.

The effect of electrode spacing, g , on G was then studied; the results are plotted in Fig. 4. Two structure widths which gave large enhancement values ($w = 50$ and 160 nm) were tested, with t_{wire} again fixed at 15 nm. The total weighted optical enhancement is plotted as a function of g , which was swept from 5 to 50 nm. Note that once the electrode spacing decreases below 10 nm for $w = 50$ nm, the value of G significantly increases due to plasmonic nanogap effects [48]. For both widths, the total weighted optical enhancement increases as gap decreases due to two main contributions. As the gap decreases: (1) the optical enhancement increases in each gap due to nanogap plasmonic effects, and (2) the density of electrode pairs increases, increasing the total current. For smaller gaps, more area of the GaAs is covered by Au, causing some reflection, absorption, or scattering of the light by the electrodes. However, this effect is much smaller than the positive effects of the other factors listed. Therefore, the net effect is an increase in optical gain within the GaAs as a function of electrode spacing. Also, since the thickness of electrodes is small, the reflection is also minimal. In general, for thicker electrodes, the reflection effect would be greater and the enhancement diminished. However, one can tune the thickness as well to optimize the signal, as shown in Ref. [48].

IV. CONCLUSION

The total weighted optical enhancement effects in a photodetector containing interdigital plasmonic electrodes were investigated by considering both the plasmonic optical enhancement and the current density within the semiconductor substrate. The simultaneous consideration of these effects was utilized to determine the total enhancement for MSM PD applications since enhanced photogeneration in regions of high current density should lead to greater overall photocurrent. The two key parameters studied were wire and nanoslit width, which greatly influence the total optical enhancement of the device. It was demonstrated that the regions of highest current density (bottom edges of the nanoscale electrodes) are near the highest optical enhancement (hotspot) regions. This can lead to a further increase in the total current of the device. To predict this increase for the proposed range of device geometries, the total optical enhancement was calculated and weighted by the local current density. The results showed that fabricating the smallest possible electrodes and electrode spacing can lead to enhancement values more than an order of magnitude greater than those for non-plasmonic devices. Optimizing the structure by decreasing the structure period and width for small, constant nanoslit widths has been demonstrated to increase the enhancement by up to two orders of magnitude compared to that of larger structures/periods. Nanoslits below 10 nm and electrode widths down to 50 nm are the predicted optimal geometric specifications to optimize device current. This work also shows that plasmonic gap enhancement effects outweigh any unwanted shadowing effect when using optically thin electrodes.

REFERENCES

- [1] E. Ozbay “Plasmonics: Merging photonics and electronics at nanoscale dimensions,” *Science*, vol. 311, no. 5758, pp. 189–193, Jan. 2006.
- [2] A. A. Darweesh, S. J. Bauman, Z. T. Brawley, and J. B. Herzog, “Improved optical enhancement in binary plasmonic gratings with nanogap spacing,” *SPIE Nanosci. Eng.*, vol. 9927, 2016, Art. no. 99270Z.
- [3] C.-C. Chang *et al.*, “A surface plasmon enhanced infrared photodetector based on InAs quantum dots,” *Nano Lett.*, vol. 10, no. 5, pp. 1704–1709, May 2010.
- [4] B. Y. Zheng, Y. Wang, P. Nordlander, and N. J. Halas, “Color-selective and CMOS-compatible photodetection based on aluminum plasmonics,” *Adv. Mater.*, vol. 26, no. 36, pp. 6318–6323, Sep. 2014.
- [5] M. W. Knight, H. Sobhani, P. Nordlander, and N. J. Halas, “Photodetection with active optical antennas,” *Science*, vol. 332, no. 6030, pp. 702–704, 2011.
- [6] J. Hetterich, G. Bastian, N. A. Gippius, S. G. Tikhodeev, G. von Plessen, and U. Lemmer, “Optimized design of plasmonic MSM photodetector,” *IEEE J. Quantum Electron.*, vol. 43, no. 10, pp. 855–859, Oct. 2007.
- [7] J. N. Munday and H. A. Atwater, “Large integrated absorption enhancement in plasmonic solar cells by combining metallic gratings and antireflection coatings,” *Nano Lett.*, vol. 11, no. 6, pp. 2195–2201, Jun. 2011.
- [8] V. E. Ferry *et al.*, “Light trapping in ultrathin plasmonic solar cells,” *Opt. Express*, vol. 18, no. 102, pp. A237–A245, Jun. 2010.
- [9] R. Yu, Q. Lin, S.-F. Leung, and Z. Fan, “Nanomaterials and nanostructures for efficient light absorption and photovoltaics,” *Nano Energy*, vol. 1, no. 1, pp. 57–72, Jan. 2012.
- [10] I. Thomann, B. A. Pinaud, Z. Chen, B. M. Clemens, T. F. Jarillo, and M. L. Brongersma, “Plasmon enhanced solar-to-fuel energy conversion,” *Nano Lett.*, vol. 11, no. 8, pp. 3440–3446, Aug. 2011.
- [11] A. Aubry, D. Y. Lei, A. I. Fernández-Domínguez, Y. Sonnefraud, S. A. Maier, and J. B. Pendry, “Plasmonic light-harvesting devices over the whole visible spectrum,” *Nano Lett.*, vol. 10, no. 7, pp. 2574–2579, Jul. 2010.
- [12] K. Nakayama, K. Tanabe, and H. A. Atwater, “Plasmonic nanoparticle enhanced light absorption in GaAs solar cells,” *Appl. Phys. Lett.*, vol. 93, no. 12, Sep. 2008, Art. no. 121904.
- [13] H. A. Atwater and A. Polman, “Plasmonics for improved photovoltaic devices,” *Nature Mater.*, vol. 9, no. 3, pp. 205–213, Mar. 2010.
- [14] K. R. Catchpole and A. Polman, “Plasmonic solar cells,” *Opt. Express*, vol. 16, no. 26, pp. 21793–21800, Dec. 2008.
- [15] G. Raschke *et al.*, “Biomolecular recognition based on single gold nanoparticle light scattering,” *Nano Lett.*, vol. 3, no. 7, pp. 935–938, Jul. 2003.
- [16] T. Chung, S.-Y. Lee, E. Y. Song, H. Chun, and B. Lee, “Plasmonic nanostructures for nano-scale bio-sensing,” *Sensors*, vol. 11, no. 11, pp. 10907–10929, Nov. 2011.
- [17] A. G. Brolo, “Plasmonics for future biosensors,” *Nature Photon.*, vol. 6, no. 11, pp. 709–713, Nov. 2012.
- [18] P. K. Jain, X. Huang, I. H. El-Sayed, and M. A. El-Sayed, “Review of some interesting surface plasmon resonance-enhanced properties of noble metal nanoparticles and their applications to biosystems,” *Plasmonics*, vol. 2, no. 3, pp. 107–118, Sep. 2007.
- [19] A. Sivanesan, E. L. Izake, R. Agoston, G. A. Ayoko, and M. Sillence, “Reproducible and label-free biosensor for the selective extraction and rapid detection of proteins in biological fluids,” *J. Nanobiotechnol.*, vol. 13, Jun. 2015, Art. no. 43.
- [20] J. Homola, “Present and future of surface plasmon resonance biosensors,” *Anal. Bioanal. Chem.*, vol. 377, no. 3, pp. 528–539, Oct. 2003.
- [21] S. J. Bauman, Z. T. Brawley, A. A. Darweesh, and J. B. Herzog, “Substrate oxide layer thickness optimization for a dual-width plasmonic grating for surface-enhanced raman spectroscopy (SERS) biosensor applications,” *Sensors*, vol. 17, no. 7, Jun. 2017, Art. no. 1530.
- [22] J. N. Anker, W. P. Hall, O. Lyandres, N. C. Shah, J. Zhao, and R. P. Van Duyne, “Biosensing with plasmonic nanosensors,” *Nature Mater.*, vol. 7, no. 6, pp. 442–453, Jun. 2008.
- [23] M. Shalaby *et al.*, “Concurrent field enhancement and high transmission of THz radiation in nanoslit arrays,” *Appl. Phys. Lett.*, vol. 99, no. 4, Jul. 2011, Art. no. 041110.
- [24] A. E. Çetin, K. Güven, and Ö. E. Müstecaplıoğlu, “Active control of focal length and beam deflection in a metallic nanoslit array lens with multiple sources,” *Opt. Lett.*, vol. 35, no. 12, pp. 1980–1982, Jun. 2010.
- [25] T. Tanemura *et al.*, “Multiple-wavelength focusing of surface plasmons with a nonperiodic nanoslit coupler,” *Nano Lett.*, vol. 11, no. 7, pp. 2693–2698, Jul. 2011.
- [26] L. Verslegers *et al.*, “Planar lenses based on nanoscale slit arrays in a metallic film,” *Nano Lett.*, vol. 9, no. 1, pp. 235–238, Jan. 2009.
- [27] K. Iwami, M. Ishii, Y. Kuramochi, K. Ida, and N. Umeda, “Ultrasmall radial polarizer array based on patterned plasmonic nanoslits,” *Appl. Phys. Lett.*, vol. 101, no. 16, Oct. 2012, Art. no. 161119.
- [28] F. Eftekhar *et al.*, “Nanoholes as nanochannels: Flow-through plasmonic sensing,” *Anal. Chem.*, vol. 81, no. 11, pp. 4308–4311, Jun. 2009.
- [29] A. De Leebeeck, L. K. S. Kumar, V. de Lange, D. Sinton, R. Gordon, and A. G. Brolo, “On-chip surface-based detection with nanohole arrays,” *Anal. Chem.*, vol. 79, no. 11, pp. 4094–4100, Jun. 2007.
- [30] M. D. Sonntag, J. M. Klinsporn, A. B. Zrimsek, B. Sharma, L. K. Ruvuna, and R. P. V. Duyne, “Molecular plasmonics for nanoscale spectroscopy,” *Chem. Soc. Rev.*, vol. 43, no. 4, pp. 1230–1247, 2014.
- [31] R. Gordon, D. Sinton, A. G. Brolo, and K. L. Kavanagh, “Plasmonic sensors based on nano-holes: Technology and integration,” *Proc. SPIE*, vol. 6959, 2008, Art. no. 695913.
- [32] T. Vo-Dinh, H.-N. Wang, and J. Scaffidi, “Plasmonic nanoprobe for SERS biosensing and bioimaging,” *J. Biophoton.*, vol. 3, nos. 1–2, pp. 89–102, Jun. 2009.
- [33] H. Im, K. C. Bantz, S. H. Lee, T. W. Johnson, C. L. Haynes, and S.-H. Oh, “Self-assembled plasmonic nanoring cavity arrays for SERS and LSPR biosensing,” *Adv. Mater.*, vol. 25, no. 19, pp. 2678–2685, May 2013.
- [34] K. C. Bantz *et al.*, “Recent progress in SERS biosensing,” *Phys. Chem. Chem. Phys.*, vol. 13, no. 24, pp. 11551–11567, Jun. 2011.
- [35] A. M. Hill, A. I. Nusir, P. V. Nguyen, O. M. Manasreh, and J. B. Herzog, “Computational electromagnetic analysis of plasmonic effects in interdigital photodetectors,” *Proc. SPIE*, vol. 9163, 2014, Art. no. 91633Q.
- [36] A. I. Nusir, A. M. Hill, M. O. Manasreh, and J. B. Herzog, “Near-infrared metal-semiconductor-metal photodetector based on semi-insulating GaAs and interdigital electrodes,” *Photon. Res.*, vol. 3, no. 1, pp. 1–4, Feb. 2015.
- [37] C. L. Tan, V. V. Lysak, K. Alameh, and Y. T. Lee, “Absorption enhancement of 980 nm MSM photodetector with a plasmonic grating structure,” *Opt. Commun.*, vol. 283, no. 9, pp. 1763–1767, May 2010.

- [38] M. Grande *et al.*, "Asymmetric plasmonic grating for optical sensing of thin layers of organic materials," *Sens. Actuators B Chem.*, vol. 160, no. 1, pp. 1056–1062, Dec. 2011.
- [39] Y. S. Jung, J. Wuenschell, H. K. Kim, P. Kaur, and D. H. Waldeck, "Blue-shift of surface plasmon resonance in a metal nanoslit array structure," *Opt. Express*, vol. 17, no. 18, pp. 16081–16091, Aug. 2009.
- [40] K.-L. Lee, P.-W. Chen, S.-H. Wu, J.-B. Huang, S.-Y. Yang, and P.-K. Wei, "Enhancing surface plasmon detection using template-stripped gold nanoslit arrays on plastic films," *ACS Nano*, vol. 6, no. 4, pp. 2931–2939, Apr. 2012.
- [41] N. Livneh *et al.*, "Highly directional emission and photon beaming from nanocrystal quantum dots embedded in metallic nanoslit arrays," *Nano Lett.*, vol. 11, no. 4, pp. 1630–1635, Apr. 2011.
- [42] K.-L. Lee, C.-W. Lee, W.-S. Wang, and P.-K. Wei, "Sensitive biosensor array using surface plasmon resonance on metallic nanoslits," *J. Biomed. Opt.*, vol. 12, no. 4, 2007, Art. no. 044023.
- [43] Y. Gao, Q. Gan, and F. J. Bartoli, "Spatially selective plasmonic sensing using metallic nanoslit arrays," *IEEE J. Select. Topics Quantum Electron.*, vol. 20, no. 3, pp. 96–101, May 2014.
- [44] COMSOL Multiphysics, v. 5.0., COMSOL AB, Stockholm, Sweden. [Online]. Available: www.comsol.com
- [45] E. D. Palik, *Handbook of Optical Constants of Solids*. Orlando, FL, USA: Academic, 1985.
- [46] P. B. Johnson and R. W. Christy, "Optical constants of the noble metals," *Phys. Rev. B*, vol. 6, no. 12, pp. 4370–4379, Dec. 1972.
- [47] S. J. Bauman, E. C. Novak, D. T. Debu, D. Natelson, and J. B. Herzog, "Fabrication of sub-lithography-limited structures via nanomasking technique for plasmonic enhancement applications," *IEEE Trans. Nanotechnol.*, vol. 14, no. 5, pp. 790–793, Sep. 2015.
- [48] Z. T. Brawley *et al.*, "Modeling and optimization of Au-GaAs plasmonic nanoslit array structures for enhanced near-infrared photodetector applications," *J. Nanophoton.*, vol. 11, no. 1, Mar. 2017, Art. no. 016017.

Authors' biographies not available at the time of publication.